

RESEARCH ARTICLE

Investigation of Static Aeroelastic Analysis and Flutter Characterization of a Slender Straight Wing

N. Rajamurugu^{1*}, Mohit Satyam², Manoj V², V. Nagendra², S. Yaknesh¹ and M. Sundararaj¹¹Department of Aeronautical Engineering, Bharath Institute of Higher Education and Research, 600073 Chennai, Tamilnadu, India

ABSTRACT - This research aims to investigate the static aeroelastic characteristics of a slender straight 2D wing using aerodynamic strip theory. The finite element method is employed to determine the wing's divergence speed and aileron effectiveness, while Galerkin's method, based on the principle of virtual work is used to obtain the influence coefficient of the straight wing. The application of aerodynamic strip theory and finite span correction is utilized to establish a correlation between elastic twist and lift coefficient. Subsequently, a computational tool in MATLAB is formulated to derive an approximate solution for the static aeroelastic equilibrium equations concerning slender straight wings. An investigation is conducted into the impact of various elastic axis positions on the divergence speed and its implications for structural integrity are analyzed. It was observed in the study that the incorporation of finite span correction into the strip theory led to a 15% augmentation in the divergence speed of the slender wing. Validation of the mathematical model of the slender wing is performed through computational analyses conducted using ANSYS software. The flutter analysis examines parameters such as the distance between the elastic and aerodynamic axes, the sweep position, and the wing span. A MATLAB code is presented in the research article to explore the influence of these parameters on the flutter speed of a slender wing. Through an investigation of the interplay between these parameters and the flutter speed, the study strives to enhance comprehension of the fundamental mechanisms governing flutter occurrence in slender wings. The current research reveals that the flutter speed is notably affected by both the eccentricity and span of the wing. Specifically, a reduction in eccentricity leads to a 1.5% enhancement in flutter speed, while increasing the sweep angle from 15 to 30 degrees for a wing with a 15ft span results in a 2.54% increase in flutter speed. Moreover, wings spanning from 5ft to 15ft exhibit a 5% rise in flutter speed. These findings offer valuable insights for the design of more efficient and stable wings.

ARTICLE HISTORY

Received : 19th Apr. 2023
Revised : 12th Jan. 2024
Accepted : 04th Apr. 2024
Published : 20th June 2024

KEYWORDS

Aeroelasticity
Divergence
Slender wing
Elasticity
Flutter

1.0 INTRODUCTION

Aeroelasticity, a multidisciplinary field, explores the complex interaction among aerodynamic, elastic, and inertial forces, significantly influencing the design of aircraft. It divides into static aeroelasticity, which concentrates on the interplay of aerodynamic and elastic forces, and dynamic aeroelasticity, which includes inertial forces in the analysis. Wing torsional divergence and control reversal are among the crucial aeroelastic phenomena, posing risks to wing integrity and control surface effectiveness, particularly ailerons [1]. The examination of static aeroelastic behavior is crucial for slender straight wings [2], impacting aerodynamic performance and flight control characteristics under stable flight conditions [3]. Numerical techniques are essential tools for modeling and examining these intricate interactions, providing precise and effective insights. Approaches such as the Finite Element method [4], Higher Order Panel method, Three-dimensional Navier-Stokes method [5], Vortex Lattice method, and Euler-Bernoulli beam theory are utilized to assess static aeroelastic issues. Recent research has emphasized that the matrix transformations of equilibrium equations enable a comprehensive analysis of wings with varied characteristics. As introduced by previous studies, the matrix-oriented approach advances the comprehension of aeroelastic problems related to straight wings [6]. Flutter, a critical consideration in the design of high-speed aircraft, significantly impacts wing parameters like skin thickness, platform, aspect ratio, and mass distribution [7]. Decreasing the wing aspect ratio and increasing the sweep angle enhance flutter speed, while strategic positioning of heavy-mass objects helps reduce flutter risks [8]. Wing torsional divergence, a common issue for straight wings, depends on factors such as torsional stiffness and twist center offset [5]. Designers often face challenges in balancing the enhancement of torsional rigidity, which increases wing divergence, with optimizing the wing structure to improve the twist center and reduce aerodynamic eccentricity [9]. As investigated by previous studies, a three-dimensional Navier-Stokes algorithm utilizing a zonal grid-generation method provides insights into the flow dynamics of complex, flexible fighter aircraft [10]. Additionally, the High-Order Panel technique [11] and modal methods, recommended by previous research [12], analyze static aeroelastic characteristics, capturing crucial parameters including pressure distribution, structural deformation, and aerodynamic coefficients. Finite elements are employed to approximate Euler/Navier-Stokes equations, demonstrating the flexibility of numerical simulations in exploring aeroelastic dynamics.

Studies relevant to flutter research suggested that to carry out the flutter characters of high aspect ratio wings the Fluid-Structure-Interaction (FSI) approach is recommended [13][14]. Employing MATLAB-based aeroelastic tailoring with radial basis function neural networks and genetic algorithms, revealing nuanced optimizations for swept-forward wings. Finite element techniques [15] are also used to study the lamination parameter to determine the flutter and divergence instabilities. Exploring fluid-structure coupling, [16] adopts the corotational approach to analyze structure, revealing that increasing bending and torsional stiffness along the wing span significantly reduces flutter amplitudes. Moreover, the study suggests that pre-twisting a wing alters flutter dynamics, providing valuable insights into flutter frequency modulation. Another avenue of exploration involves the integration of flutter and divergence responses into the weight optimization framework, utilizing the level set approach for wing topology optimization [17]. Recent studies [18][19] on the static and dynamic analysis of flexible, rigid, composite laminate plates have thrown light on the advancement of codes [20] and experimental techniques. Several studies on the nonlinear nature of the wings [21][22] under given dynamic conditions also gave a valuable torch to the simulation studies. An extensive study on the oscillating airfoil [23], forward swept wings with pre-twist [24], aeroelastic problems of high aspect ratio wings, and multi-element airfoil have been carried out in the past with reliable solutions. This research paper's primary objective is to unravel the static aeroelastic behavior of slender straight wings through a comprehensive numerical and computational approach. Forward-swept wing aeroelastic behavior is studied [25] by a medium-fidelity model to predict wing displacements, with good agreement between the model and wind tunnel tests presented. A reduced-order model for a flexible wing undergoing stall flutter, based on structural kinematic measurements [26], was further refined [27] for predicting loads generated by a flexible flapping wing. A non-intrusive optical technique was used to measure wing deformation. A study delved into the higher frequency aspects of stall flutter, pinpointing the fifth harmonic as being associated with the frequency of dynamic stall vortex shedding. Building upon this research [28], further investigation led to the development of a streamlined model for dynamic stalls. This was accomplished through the utilization of a fuzzy inference system and orthogonal functions, resulting in highly accurate modeling of aerodynamic response. These studies collectively contribute to the understanding and prediction of stall flutter in flexible wings. In the present work a proposed model, grounded in St. Venant torsion theory, aims to yield accurate predictions of aeroelastic properties, encompassing spanwise lift distribution, control effectiveness, tip deflection, and dynamic pressure across various Mach numbers. By advancing a robust numerical model, the study strives to contribute to the development of safer and more efficient aircraft structures. The paper systematically unfolds the theory behind static aeroelastic characteristics, organized into three sections, offering solutions via strip theory for distinct scenarios. The second section presents a numerical example and results derived from a MATLAB program [29]. The third section adopts a computational fluid dynamic (CFD) based analysis, probing tip displacement, lift coefficient, and torsion angle at diverse span locations. This multifaceted exploration promises a nuanced understanding of the static aeroelastic behaviors of slender straight wings, fostering advancements in aircraft design and safety.

2.0 THEORY OF SLENDER WING

The elastic axis of the designed Slender straight wings can be characterized by the assumption that the elastic axis needs to be perpendicular to the plane of symmetry of the aircraft. In such wings, aeroelastic phenomena entirely depend upon wing twists about the elastic axis and wing bending is not a factor. It is also assumed that the chordwise segment of the wing is rigid, so the bending is neglected. The equilibrium equation for torsional aeroelasticity in a straight wing, concerning the rate of twist and the applied torque, is derived by applying the St. Venant torsion theory.

$$\frac{d}{dy} \left(GJ \frac{d\theta}{dy} \right) = -t(y) \tag{1}$$

$$T(y) = (ecc_1 + c^2c_{mac})q - Nmgd \tag{2}$$

The equilibrium equation in its differential form is derived by substituting the torque per unit span into the previously mentioned equation.

$$\frac{d}{dy} \left(GJ \frac{d\theta}{dy} \right) - (ecc_1 + c^2c_{mac})q - Nmgd \tag{3}$$

$$\frac{d}{dy} \left(GJ \frac{d\theta}{dy} \right) + qe ecc_l = qc^2c_{mac} + Nmgd \tag{4}$$

The deflection due to bending can be written as,

$$\theta(y) = \int_0^l c^{\theta\theta}(y, \eta) [(ecc_1 + c^2c_{mac})q - Nmgd] d\eta \tag{5}$$

By superpositioning the rigid angle of attack and elastic twist the resultant angle of attack is given by

$$\alpha(y) = ar(y) + \theta(y) \tag{6}$$

Like how the lift coefficient and elastic lift coefficient are combined to form the local lift coefficient

$$C_l(y) = C_l^r(y) + C_l^e(y) \tag{7}$$

Substituting the values in (3)

$$\frac{d}{dy} \left(GJ \frac{d\theta}{dy} \right) + qe ecc_l = ecc_l^r - qc^2 c_{mac} + Nmgd \tag{8}$$

$$\theta(y) = q \int_0^l c^{\theta\theta}(y, \eta) (ecc_{c1} + c^2 c_{mac}) + f(y)$$

where

$$f(y) = \int_0^l c^{\theta\theta}(y, \eta) ((qecc_l^r + qc^2 c_{mac} - Nmgd) d\eta$$

The equilibrium differential equation has been extensively utilized to solve simplified problems. In this context, $\theta(y)$ and $c_l e(y)$ are treated as unknown functions while the other terms are defined. Providing the relation between these two will make the problem mathematically determinate. This is achieved by adopting the suitable aerodynamic theory. In our scenario, the linear aerodynamic theory has been employed, where there exists a linear correlation between the angle of incidence and lift distribution, expressed as

$$\alpha(y) = A[ccl] \tag{9}$$

Recent advancements in the aeroelasticity of straight wings have led to innovative methods for transforming the equilibrium differential equation into a matrix representation, where A is a linear operator acting on the lift distribution to generate the desired incidence distribution. These techniques provide an upper edge in depicting the wing with nonuniform properties.

2.1 Solution using Strip theory

Strip theory is a simplification technique employed to evaluate the aerodynamic behavior of a 2D wing. This approach posits that the wing can be segmented into multiple rectangular strips, each characterized by a constant chord and varying circulation along the span [17,30]. However, simplification comes at a cost of accuracy and may not provide accurate results for all aircraft types and operating conditions. It also assumes that the wing is uniformly loaded, which may not be true for real aircraft, which can experience localized loading due to factors such as gusts, control surface deflections, and wing-fuselage interactions.

Since both $\theta(y)$ and c_l^e are unknown functions in equation (8), according to the aerodynamic theory, the angle of impact and lift distribution have a linear relationship that may be expressed by

$$\alpha(y) = \theta(ccl)$$

$$\theta = \frac{1}{a_0 c} \tag{10}$$

The lowest Eigenvalue of dynamic pressure q_d was obtained from the integration of a homogenous equilibrium equation to compute the torsional divergence speed of a three-dimensional wing. Hereby, the Equation (8)'s homogeneous form is as follows:

$$\frac{d}{dy} \left(GJ \frac{d\theta}{dy} \right) + q_d c e c_l^e = 0 \tag{11}$$

$$\theta(y) = q_d \int_0^l c^{\theta\theta}(y, \eta) ecc_l^e d\eta$$

The integral equation (11) using strip theory:

$$\frac{c_l^e}{\frac{dc_l}{d\alpha}} = q_d \int_0^l c^{\theta\theta}(y, \eta) ecc_l^e d\eta$$

The aerodynamic operator A can be represented as,

$$A = \frac{1}{a_0 c} \tag{12}$$

The differential equation of equilibrium in matrices form can be arranged as,

$$[A]\{cc_e^l\} = q_d [E]\{cc_e^l\}, \tag{13}$$

where $A = \frac{1}{\frac{dc_l}{d\alpha}} \left[\frac{1}{c} \right]$

$E = [C^{\theta\theta}] [e][W]$, where $[W]$ = Weighted matrix. To obtain the non-zero solution of c_e^l

$$[A] - q[E] = 0 \tag{14}$$

The minimum Eigenvalue of the matrix [A] corresponds to the dynamic pressure at which divergence occurs. The divergence speed can then be determined through further calculations involving;

$$q_d = \frac{1}{2} \rho v_d^2 \tag{15}$$

where v_d is the divergence speed. Further, the influence coefficient $C^{\theta\theta}$ at different stations can be obtained using the following equation:

$$C^{\theta\theta}(y, \eta) = \int_0^y \frac{d\lambda}{GJ}$$

$$C^{\theta\theta}(y, \eta) = \int_0^n \frac{d\lambda}{GJ} \tag{16}$$

To investigate the variation of wing twist with speed, the nondimensional parameters “q/qd” (the ratio of dynamic pressure to divergence dynamic pressure) and “U/Ud” (the ratio of speed to divergence speed) are plotted against θ/θ_r . The equation for the elastic twist is given as

$$\theta = \frac{c^{\theta\theta} \left[\left(\frac{\partial C_L}{\partial \alpha} \right) e\alpha^r + C_{MAC} c \right] qS}{1 - c^{\theta\theta} \left(\frac{\partial C_L}{\partial \alpha} \right) qS e} \tag{17}$$

and for cases where the twist doesn't introduce any additional aerodynamic load the elastic twist can be obtained by putting the AOA $\alpha = \alpha_r$ and given as

$$\theta_r = c^{\theta\theta} \left(\frac{\partial C_L}{\partial \alpha} e\alpha^r + C_{MAC} c \right) qS \tag{18}$$

The equilibrium equations, which relate the rate of twist to applied torque, were solved using MATLAB by inputting the necessary geometric and aerodynamic parameters to determine the lowest Eigenvalue of dynamic pressure. For slender straight wings, the divergence speed was computed using strip theory with and without finite span correction and lifting-line theory for both symmetric and antisymmetric cases. The obtained divergence speeds from the MATLAB code were compared with reference results for each scenario. Appendix A contains the MATLAB program. The position of the elastic axis is a crucial parameter influencing the wing's divergence speed. When the elastic axis shifts away from the aerodynamic center, the wing becomes more flexible, leading to a decrease in torsional stiffness and consequently, a reduction in the divergence speed. To examine the impact of the elastic axis position on divergence speed, the code can be adjusted to vary the elastic axis location from 0.30c to 0.50c in increments of 0.5c.

2.2 Static Aeroelastic Analysis Solution Using MATLAB

The wing is segmented into four stations along the half-span, also known as Multhopp's stations. It's assumed that the elastic axis is straight and positioned at 35% of the chord. A torque is applied at a distance n from the origin, resulting in an angular displacement $C^{\theta\theta}$ at the point y.

Table 1. Geometrical parameters of a slender straight wing

Geometrical Parameters	Values
Semi-span (b/2)	12.7m
Root chord (Cr)	5.71m
Tip chord (Ct)	2.54m
Wing Area	1.25sq.m
Aspect-ratio (AR)	2.90
Elastic axis (0.35c)	2m
Aerodynamic axis (0.25c)	1.42m
Sweep angle (Λ)	0
Length of the aileron ($\sqrt{l_a}$)	2.97m

The mathematical model requires geometrical configurations and design parameters as input to further develop the equilibrium equations and obtain the solutions. Computer-aided design (CAD) software has been used to construct the wing model geometry using R.L. Bisplinghoff's [30] wing design shown in Table 1. For slender straight wing configuration, NACA 0012 airfoil is selected and geometry is constructed using AUTOCAD V5 and aeroelastic analysis has been performed to obtain the divergence speed, spanwise lift distribution, and aileron effectiveness.

2.3 Governing equations for Slender straight wing for Flutter analysis

The P-k method is a classical approach to flutter analysis that involves solving the equations of motion for the wing structure and the unsteady aerodynamic loads. The method assumes that the wing structure can be modeled as a linear

system and that a set of harmonic functions can represent the unsteady aerodynamic loads. The equations of motion for the wing structure can be written as:

$$Mq'' + Cq' + K * q = F \tag{19}$$

where M is the mass matrix, C is the damping matrix, K is the stiffness matrix, q is the displacement vector, and F is the external force vector. The mass matrix represents the mass of the wing structure and is diagonal. The damping matrix represents the damping forces in the wing structure and is proportional to the velocity of the nodes. The stiffness matrix represents the stiffness of the wing structure and is calculated using the finite element method.

The p-k method is a numerical technique used to solve for the natural frequencies and mode shapes of a structure. It is based on the principle that the dynamic behavior of a structure can be described by a set of differential equations, which relate the forces applied to the structure to the resulting displacements. To solve these differential equations, the stiffness matrix (p) and the mass matrix (k) of the structure need to be determined. The stiffness matrix describes the relationship between the forces applied to the structure and the resulting displacements, while the mass matrix describes the distribution of mass within the structure. The stiffness matrix is defined as:

$$K = \int \int \int V B^T C B dV \tag{20}$$

where V is the volume of the structure, B is the strain-displacement matrix, and C is the constitutive matrix that relates stress to strain. The strain-displacement matrix B is defined as:

$$B = [B_1 B_2 \dots B_N] \tag{21}$$

where B_i is the strain-displacement matrix for the ith element in the structure. The constitutive matrix C is defined as:

$$C = [C_1 C_2 \dots C_N] \tag{22}$$

where C_i is the constitutive matrix for the ith element in the structure. The mass matrix is defined as:

$$M = \int \int \int V \rho N^T N dV \tag{23}$$

where ρ is the density of the material, N is the shape function matrix, and the integral is taken over the volume of the structure. The shape function matrix N is defined as:

$$N = [N_1 N_2 \dots N_N] \tag{24}$$

where N_i is the shape function matrix for the element in the structure.

Using the p-k method to solve a generalized eigenvalue problem. This involves finding the eigenvalues and eigenvectors of a matrix equation, where the eigenvalues represent the natural frequencies of the structure and the eigenvectors represent the corresponding mode shapes. The generalized eigenvalue problem can be written as:

$$[K - \lambda M]x = 0 \tag{25}$$

where λ is the eigenvalue and x are the eigenvector. The eigenvalues λ represent the natural frequencies of the structure, while the eigenvectors x represent the corresponding mode shapes.

To solve the generalized eigenvalue problem, assemble the stiffness and mass matrices from the element stiffness and mass matrices. This involves summing the contributions from each element in the structure. The element stiffness matrix K_e for a typical element can be written as:

$$K_e = \int \int \int V_e B^T C B dV_e$$

where V_e is the volume of the element. The element mass matrix M_e for a typical element can be written as:

$$M_e = \int \int \int V_e \rho N^T N dV_e \tag{26}$$

where ρ is the density of the material and N is the shape function matrix for the element.

The utilization of a numerical approach such as the Lanczos algorithm or the Arnoldi algorithm can be applied to solve the generalized eigenvalue problem. The Lanczos algorithm, as an iterative technique, constructs a series of Krylov subspaces that are defined by the eigenvectors of matrix A and vector b. Similarly, the Arnoldi algorithm, another iterative method, generates a sequence of Krylov subspaces but employs a distinct orthogonalization process. The resulting eigenvectors and eigenvalues correspond to the inherent frequencies and modal shapes of the system, respectively. These outcomes enable the examination of the structural dynamic response under various loading scenarios.

2.4 Theodorsen Aerodynamics

The method proposed by Theodorsen is a computational approach utilized for the determination of fluctuating aerodynamic forces acting on an airfoil. This method relies on the principle of a "quasi-steady" flow regime [31], where the unsteady airflow surrounding the airfoil is represented as a sequence of steady flows. Such an approximation remains applicable for minor oscillations of the airfoil, characterizing the unsteady flow as a disturbance to the steady flow.

Execution of the Theodorsen method necessitates the computation of aerodynamic coefficients corresponding to various reduced frequencies of the airfoil. These reduced frequencies are established as the multiplication of the oscillation frequency and the airfoil's chord length, divided by the velocity of the free stream.

The determination of aerodynamic coefficients is accomplished through the utilization of the Theodorsen function, a function with complex values that elucidates the unsteady lift and drag forces acting on the airfoil. The Theodorsen function is defined as:

$$F(\alpha, k) = C(\alpha) + iS(\alpha) + k[C'(\alpha) + iS'(\alpha)] \tag{27}$$

where α is the angle of attack of the airfoil, k is the reduced frequency, $C(\alpha)$ and $S(\alpha)$ are the real and imaginary parts of the steady-state lift coefficient, and $C'(\alpha)$ and $S'(\alpha)$ are the real and imaginary parts of the unsteady lift coefficient. The steady-state lift coefficient $C(\alpha)$ and drag coefficient $D(\alpha)$ can be calculated using the classical thin airfoil theory, which assumes that the airfoil is infinitely thin and has a symmetric cross-section. The lift and drag coefficients are given by:

$$\begin{aligned} F C_L(\alpha) &= 2\pi\alpha \\ C_D(\alpha) &= 0 \end{aligned} \tag{28}$$

where α is the angle of attack of the airfoil. The unsteady lift coefficient $C'(\alpha)$ and drag coefficient $D'(\alpha)$ can be calculated using the Theodorsen function. The unsteady lift coefficient is given by:

$$C_L'(\alpha) = 2\pi F'(\alpha, k) \tag{29}$$

where $F'(\alpha, k)$ is the derivative of the Theodorsen function concerning α . The unsteady drag coefficient is given by:

$$C_D'(\alpha) = 2\pi \text{Im}[F'(\alpha, k)] \tag{30}$$

where $\text{Im}[F'(\alpha, k)]$ denotes the imaginary part of the complex number. The Theodorsen function can be calculated using a numerical integration method, such as Simpson's rule or the trapezoidal rule. The resulting values of the Theodorsen function can be used to calculate the aerodynamic coefficients of the airfoil for a range of reduced frequencies. The Theodorsen function can be expressed in terms of the Kutta-Joukowski function, which describes the lift generated by a two-dimensional airfoil in an incompressible flow. The Kutta-Joukowski function is given by:

$$K(\alpha) = 2\pi i\alpha \tag{31}$$

The Theodorsen function can be written as:

$$F(\alpha, k) = K(\alpha) + kG(\alpha, k) \tag{32}$$

where $G(\alpha, k)$ is a complex-valued function that describes the unsteady effects on the lift and drag coefficients. The function $G(\alpha, k)$ can be expressed as a Fourier series in terms of the reduced frequency k :

$$G(\alpha, k) = \sum_{n=1}^{\infty} g_n(\alpha) e^{-ink} \tag{33}$$

where $g_n(\alpha)$ is a complex-valued function that depends on the angle of attack α . The coefficients $g_n(\alpha)$ can be calculated using the method of matched asymptotic expansions, which involves matching the solutions of the unsteady flow equations in the near-field and far-field regions of the airfoil. The resulting values of the Theodorsen function can be used to calculate the aerodynamic coefficients of the airfoil for a range of reduced frequencies. The aerodynamic coefficients can be expressed in terms of the Theodorsen function as:

$$\begin{aligned} C_L &= 2\pi F(\alpha, k) \\ C_D &= 2\pi \text{Im}[F(\alpha, k)] \end{aligned} \tag{34}$$

where C_L is the lift coefficient, C_D is the drag coefficient, and $\text{Im}[F(\alpha, k)]$ denotes the imaginary part of the complex number.

2.5 Flutter analysis by P-k method and Theodorsen aerodynamics for two-degree-of-freedom

By considering a two-degree-of-freedom system, which consists of two masses connected by springs and dampers. The system is subject to aerodynamic forces, which depend on the relative motion of the masses. The equations of motion for this system are as follows [32]:

$$\begin{aligned} m_1 x_1'' + c_1 x_1' + k_1 x_1 + k_2(x_1 - x_2) &= f_1 \\ m_2 x_2'' + c_2 x_2' + k_2(x_2 - x_1) &= f_2 \end{aligned} \tag{35}$$

Here, x_1 and x_2 are the displacements of the two masses, m_1 and m_2 are their masses, c_1 and c_2 are their damping coefficients, k_1 and k_2 are their spring constants, and f_1 and f_2 are the aerodynamic forces acting on the masses. To analyze the flutter behavior of this system, assume that the motion of the masses can be represented by a combination of two modes of vibration, which we call the "p" mode and the "k" mode. The p mode represents the motion of the two masses in phase, while the k mode represents the motion of the two masses out of phase. The displacement of each mass in terms of these modes is as follows:

$$\begin{aligned} X_1 &= A_p \cos(w_p t) + A_k \cos(w_k t) \\ X_2 &= A_p \cos(w_p t) - A_k \cos(w_k t) \end{aligned} \tag{36}$$

Here, A_p and A_k are the amplitudes of the p and k modes, respectively, and w_p and w_k are their natural frequencies. Note that the p mode has the same displacement for both masses, while the k mode has opposite displacements for the two masses. Substituting these expressions into the equations of motion and simplifying,

$$\begin{aligned} (-m_1 w_p^2 - k_1 - k_2) A_p + k_2 A_p &= \frac{f_1}{m_1} \\ k_2 A_k + (-m_2 w_p^2 - k_2) A_k &= \frac{f_2}{m_2} \end{aligned} \tag{37}$$

These equations in matrix form are as follows:

$$\begin{aligned} [(-m_1 w_p^2 - k_1 - k_2) \ k_2] [A_p] &= \left[\frac{f_1}{m_1} \right] \\ [k_2 \ (-m_2 w_p^2 - k_2)] [A_k] &= \left[\frac{f_2}{m_2} \right] \end{aligned} \tag{38}$$

The determinant of the matrix is given by:

$$\det = (-m_1 w_p^2 - k_1 - k_2)(m_2 w_p^2 - k_2) - k_2^2 \tag{39}$$

If the determinant is zero, then the system has a non-trivial solution, which corresponds to the flutter mode. Setting the determinant to zero and solving for w_p^2 ,

$$(m_1 m_2 w_p^4 + (m_1 c_2 + m_2 c_1) w_p^3 + ((k_1 + k_2) m_2 + k_2 m_1) w_p^2 + (c_1 k_2 + c_2 k_1) w_p + k_1 k_2) = 0 \tag{40}$$

This is the characteristic equation for the system, which provides the natural frequencies of the system. The roots of this equation yield the natural frequencies, which are associated with the flutter speed. To solve for the flutter speed, we set the real part of the natural frequencies to zero, as flutter manifests when the real part of the frequency becomes positive. This gives us the following equation:

$$(m_1 m_2) w^4 + (m_1 c_2 + m_2 c_1) w^3 + (((k_1 + k_2) m_2 + k_2 m_1) w^2 + (c_1 k_2 + c_2 k_1) w + k_1 k_2) = 0 \tag{41}$$

Here, w is the natural frequency of the system, which is related to the flutter speed by the following equation:

$$v_f = w \sqrt{\frac{m_1 + m_2}{k_1}} \tag{42}$$

This equation gives us the flutter speed in terms of the natural frequency and the masses and spring constant of the system.

2.7 Static Aeroelastic Analysis- Ansys FSI Oriented Approach

The achieved outcome is further verified through the execution of CFD analysis within the ANSYS FSI framework. An illustration in Figure 1 illustrates the sequential process of the examination in Ansys. The analysis of static aeroelasticity is a crucial method employed in the field of aerospace engineering for exploring the relationship between aerodynamic forces and the structural response of an aircraft. The primary objective of this examination is to ascertain the ability of the aircraft's design to endure the pressures and distortions encountered during operation. To accomplish this objective, engineers utilize simulation tools such as ANSYS for conducting a Finite Element Analysis (FEA) combined with Computational Fluid Dynamics (CFD) analysis.

In the realm of Fluid-Structure Interaction (FSI) methodology, the analyses of Finite Element Analysis (FEA) and Computational Fluid Dynamics (CFD) are interconnected in such a manner that facilitates the transfer of data between the respective domains. This signifies the consideration of structural deformation within the CFD analysis, alongside the incorporation of aerodynamic forces within the FEA analysis. Through the iterative process of these analyses, scholars can achieve a heightened level of precision in forecasting the performance of an aircraft. The present investigation employed ANSYS software to delineate the three-dimensional geometry of a wing encompassing both the solid structural component and the fluidic region. Utilizing the meshing capabilities of ANSYS, a detailed mesh was generated for both the wing structure and fluidic domain, subsequently applying diverse boundary conditions, such as inflow velocity and pressure. The FSI assessment was carried out employing an integrated solver, enabling real-time interaction between the fluid and structural domains. The aerodynamic configuration entailed a slender straight wing featuring a NACA 0012 airfoil and a taper ratio of 0.44. The fluid domain was characterized by a length of 10c and a width of 2b, exhibiting symmetry on one side and no-slip walls on the remaining three boundaries.

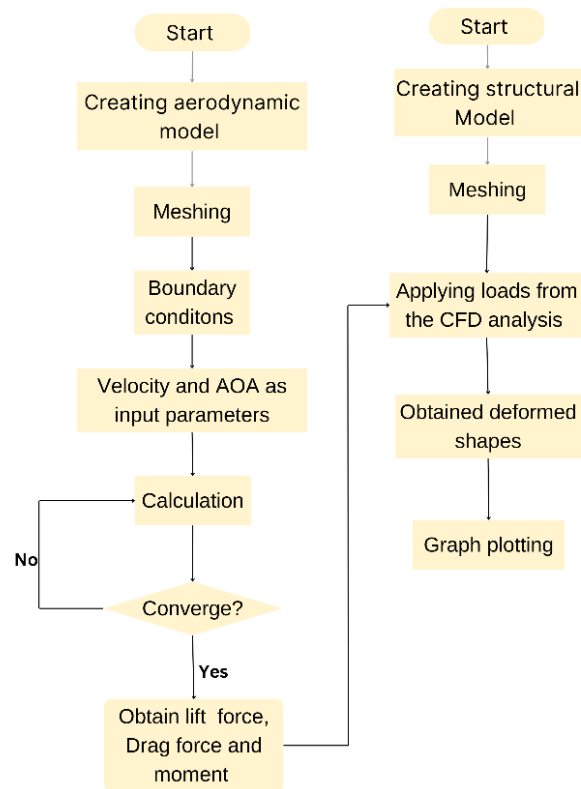


Figure 1. The Flow chart of design analysis in ANSYS

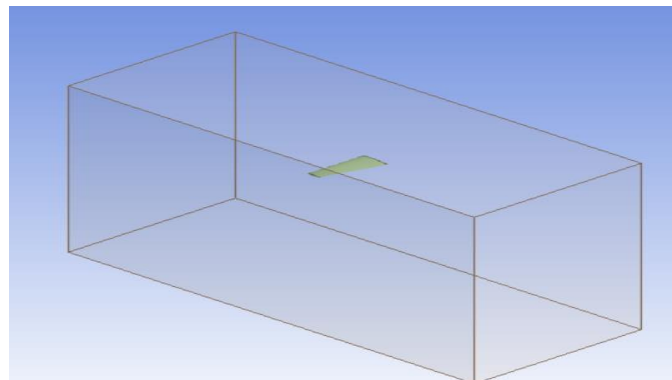


Figure 2. Fluid domain for Aerodynamic analysis

The process of mesh generation within ANSYS, a widely utilized software for CFD), plays a crucial role in precisely capturing the intricate geometry and physical phenomena of a simulation domain. This process is essential for achieving dependable and accurate simulation outcomes. It involves the partitioning of the continuous geometry of the problem domain into a finite quantity of interconnected elements or cells, generating a numerical grid that depicts the computational domain, as illustrated in Figure 2. Various meshing techniques like structured, unstructured, and hybrid approaches can be employed based on the particular requirements of the simulation, such as the complexity of the geometry, flow characteristics, and numerical precision. In order to circumvent issues like numerical diffusion, gradient smearing, and numerical instabilities, it is imperative to assess and enhance mesh quality, which encompasses factors like element size, aspect ratio, skewness, and smoothness. Mesh sensitivity analysis can also be used to evaluate the mesh dependency of the results and ensure convergence. A Computational fluid dynamic mesh (Figure 3) with linear element order is used. The details of the domain and other computational input parameters details are presented in Table 2. In this study, a pressure-based analysis is conducted on a NACA 0012 wing configuration with a velocity inlet, pressure outlet, and no-slip walls. The analysis employs a pressure velocity coupling solution method with a second-order pressure method and momentum and first-order upwind equation for modified turbulent viscosity. To determine the generalized forces under various Mach numbers and deflections, a model is utilized.

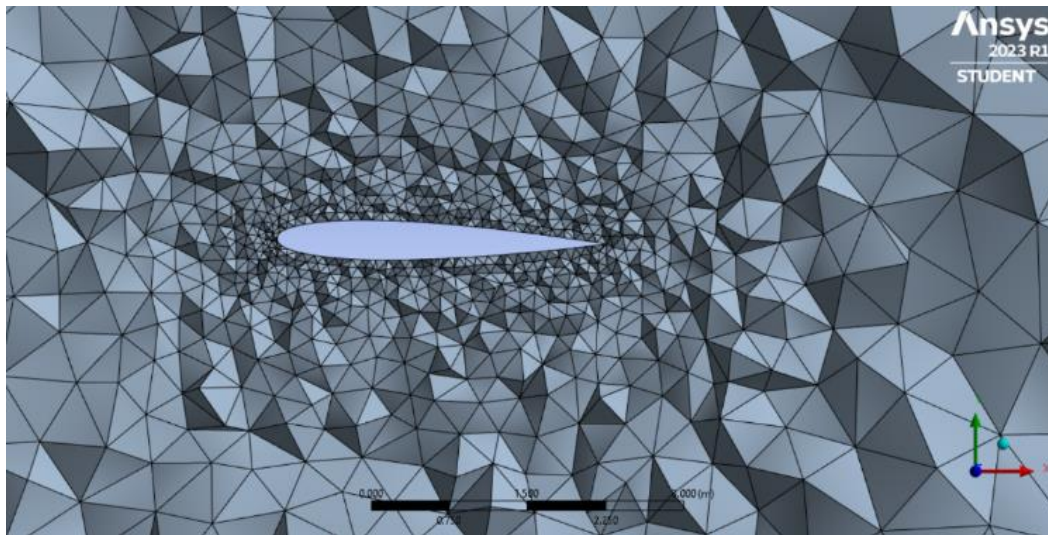


Figure 3. Wing meshing with a NACA 0012 airfoil with a fluid domain

The model requires the inputs of generalized displacements, Mach number, and angle of attack. The resulting output is a set of generalized force coefficients.

Table 2. Geometrical parameters of a slender straight wing

Parameter	Value
Grid Levels	Coarse, Medium, Fine
Number of Cells (Coarse)	625,000
Number of Cells (Medium)	1,036,800
Number of Cells (Fine)	1,423,200
Grid Refinement	Coarse → Medium → Fine
Nondimensional Wall Distance ($\delta < 1$)	Ensured for all cases
Governing Equations	Reynolds-Averaged Navier-Stokes
Discretization Method	Conservative, Time-Implicit FVM
Turbulence Model	SST Two-Equation
Density-Based Solver	Yes
Constant Flow Density	Yes
Inlet Boundary Condition	Velocity Inlet
Mesh Updating Method	Diffusion-Based Smoothing
Lift Force Calculation	Conducted for Grid Convergence Test
Medium and Fine Grid Results Agreement	Excellent for Increasing Flow Dynamic Pressure
Maximal Difference (Medium vs. Fine Grids)	Noteworthy
Optimal Grid Level for Analysis	Medium
Structural Mesh Elements	3D 20-node Solid Elements (2400 elements)

This table.2 summarizes the key parameters and results of the CFD analysis for the slender straight wing. The grid levels, cell counts, boundary layer resolution, solver settings, and mesh characteristics are detailed, emphasizing the convergence test conducted on the lift force. The agreement between medium and fine grid results, along with the maximal difference, supports the conclusion that the medium-level grid is deemed sufficient for the subsequent analysis (Figure 4). The structural mesh is composed of 2400 3D 20-node solid elements, ensuring a comprehensive representation of the wing's structural aspects.

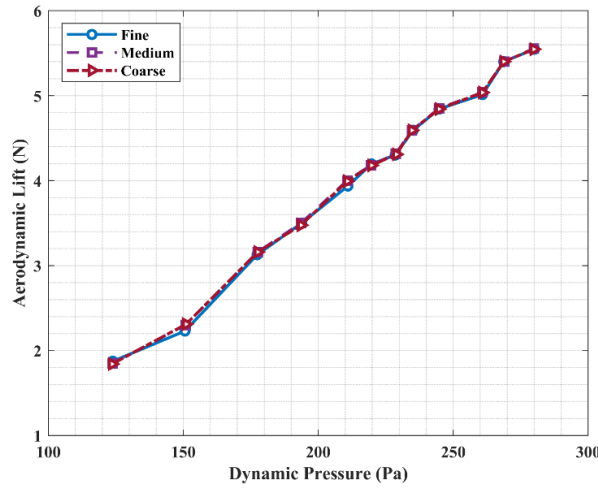


Figure 4. Mesh independency study

The functional relationship between the inputs and outputs is denoted as

$$f = f_{gf} (Ma, AOA, \xi) \tag{43}$$

where f denotes the vector of generalized force coefficients and denotes the vector of generalized displacements. Because the coefficients are nondimensionalized by the dynamic pressure, f must be multiplied by the dynamic pressure to obtain the generalized forces. The forces would be used to calculate the wing's deformation, which would be used to advance the procedure. This model will be called many times during the static aeroelastic analysis to replace the CFD flow solver [25]. The model was used to develop the Lift and drag coefficients of a wing. The concrete function can be written as

$$C_L, C_D T = f (Ma, \xi),$$

A finite element model was developed to investigate the structural behavior of a wing subjected to varying lift and drag forces. The finite element analysis (FEA) technique was employed to discretize the wing into smaller elements and analyze their interplay using the finite element method (FEM). Specifically, beam element shape functions were utilized in the FEA model to estimate the displacement field within each beam element. The beam elements, commonly employed in modeling slender structures undergoing bending and axial loads, were assumed to exhibit small deformations and linear elasticity, to derive the corresponding shape functions.

The shape functions of a typical Euler-Bernoulli beam element with 5 nodes are shown below.

$$N1 = (1 - \xi)^4(1 + \xi) \tag{44}$$

$$N2 = (1 - \xi)^3(1 + \xi)^2 \tag{45}$$

$$N3 = (1 - \xi)^2(1 + \xi)^3 \tag{46}$$

$$N4 = (1 - \xi)^1(1 + \xi)^4 \tag{47}$$

$$N5 = (1 + \xi)^5 \tag{48}$$

where ξ is the local coordinate along the length of the beam element, ranging from -1 to 1, with -1 indicating the start node and 1 indicating the end node. The shape functions $N1, N2, N3, N4,$ and $N5$ correspond to the nodal displacements at the element nodes. $N1$: This shape function represents the variation of the displacement field at the beam element's start node. The fourth-order polynomial function vanishes at the boundaries of the beam (-1 and 1) and reaches its peak at the initial node (-1). $N2$: This particular shape function illustrates the fluctuation of the displacement field at the second node of the beam element. It is characterized by a fifth-order polynomial equation with a peak at the node $-2/3$ and $2/3$ and a vanishing point at the beam's boundaries (-1 and 1). $N3$: The shape function corresponding to the third node of the beam element depicts the changes in the displacement field. It is described by a fifth-order polynomial function that attains a maximum value at the node $-1/3$ and $1/3$ while reaching a minimum at the boundaries of the beam (-1 and 1). $N4$: The shape function associated with the fourth node of the beam element represents the fluctuations in the displacement field. It is characterized by a fifth-order polynomial function that peaks at node 0 and reaches a minimum at the beam's boundaries (-1 and 1). $N5$: This shape function illustrates the variations in the displacement field at the terminal node of the beam element. It is a fifth-order polynomial function with peaks at the end nodes ($= -1$ and $= 1$) and a disappearance in the middle of the beam ($= 0$).

3.0 RESULTS AND DISCUSSIONS

Figure 5 shows that there is a decrement in the velocity ratio and the dynamic pressure ratio with an increment in the twist ratio. This implies that at higher values of twist, the wing reaches its divergence speed and dynamic pressure earlier compared to lower values of twist. This is because the increased twist causes a reduction in the wing's stiffness, leading to greater deformation under aerodynamic loads, and also increases the aerodynamic forces acting on the wing. Also, this plot shows that the nondimensional speed and dynamic pressure ratios reach a minimum value at a certain nondimensional twist parameter, indicating that there is an optimum twist value at which the wing operates most efficiently. From Table 3, it's evident that strip theory with finite span correction provides a more conservative or accurate result compared to the case without finite span correction. In the absence of finite span correction, the divergence speed lacks practical significance; however, it can still offer insight into the relative order of divergence speed for a specific slender straight wing.

Table 3. Validation of the present study

Method of Analysis: Strip theory	Present Study	Reference [6]
Without finite span correction $\frac{dc_l}{d\alpha} = 5.5$	462.14 m/s	462.25 m/s
with finite span correction $\frac{dc_l}{d\alpha} = 4.5$	532.11 m/s	532.15 m/s

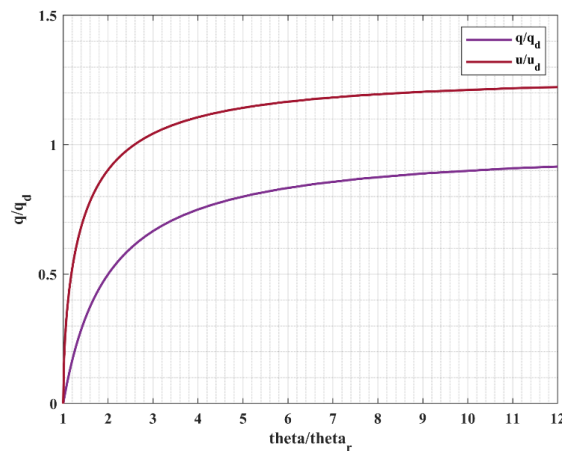


Figure 5. Variation of nondimensional twist parameter with speed

The results are plotted in Figure 6 to show the effect of the position of the elastic axis on the divergence speed. The plot will show that as the elastic axis moves away from the aerodynamic center, the divergence speed decreases. This is due to the reduction in torsional stiffness resulting from the increased flexibility of the wing.

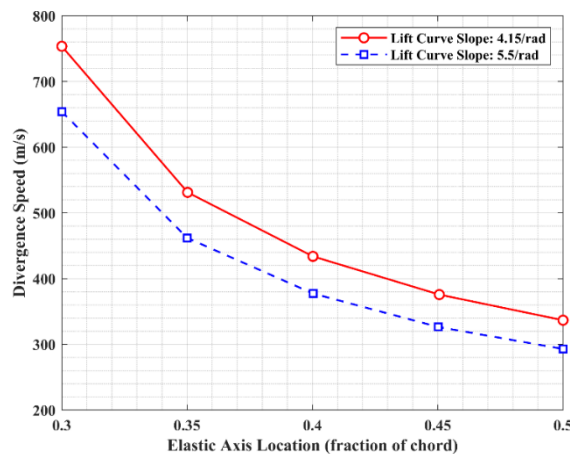


Figure 6. Effect of elastic axis location on divergence speed

Hence, careful selection of the elastic axis location is crucial to ensure the wing possesses adequate stiffness to withstand torsional deformation and attain the desired level of performance. It can be observed from Figure 7 that increment in Mach number, the effectiveness of control surfaces decreases due to the increasing compressibility effects. This is because the shock waves that form around the control surface can disrupt the flow and reduce the lift generated by the control surface. In addition, at transonic speeds, where the airflow around the aircraft is a combination of subsonic and supersonic flows, the effectiveness of control surfaces can be highly dependent on the specific design of the control surface and its location on the aircraft.

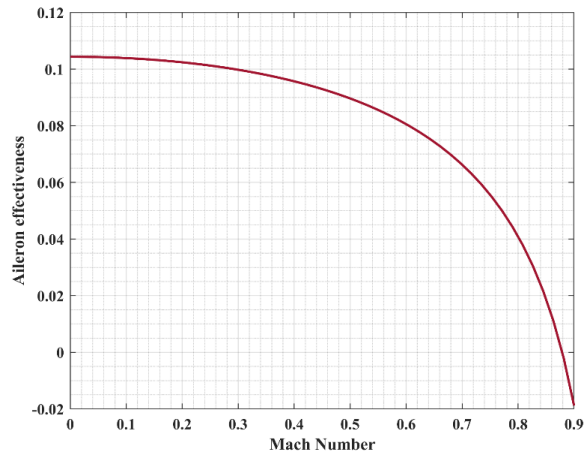


Figure 7. Aileron effectiveness with speed

The present study presents a graphical analysis of the relationship between an aircraft's lift coefficient (C_L) and wing span in Figure 8. The lift coefficient is a dimensionless quantity that characterizes the lift production capability of an aircraft wing, while the wing span is the distance between the wingtips. The results indicate that, at a speed of 532m/s, the lift from the root increases along the span up to the mid-span and then gradually decreases, primarily due to the influence of surface area and flexibility factors. Additionally, Figure 9 provides insight into the variation of tip deflection with dynamic pressure. It is well-established that dynamic pressure is directly proportional to the altitude and velocity, resulting in increased wing tip deflection with an increase in dynamic pressure. It is seen that deflection increases along the span linearly due to the distribution of bending moments along the beam causing the deflection to be greater at the tip than at the root. This is due to the higher bending moment at the fixed end causing a larger bending deformation and thus a greater deflection at that end.

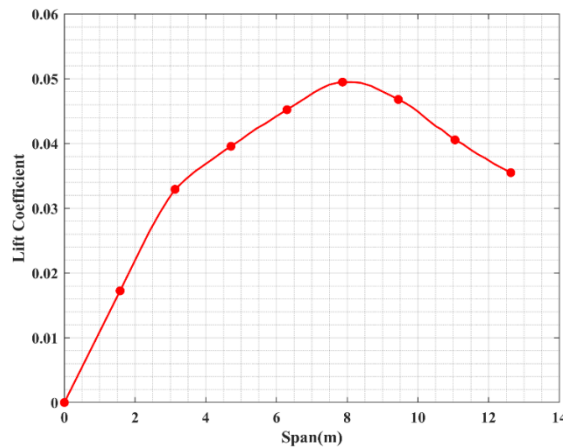


Figure 8. Lift coefficient along the span for slender straight-wing

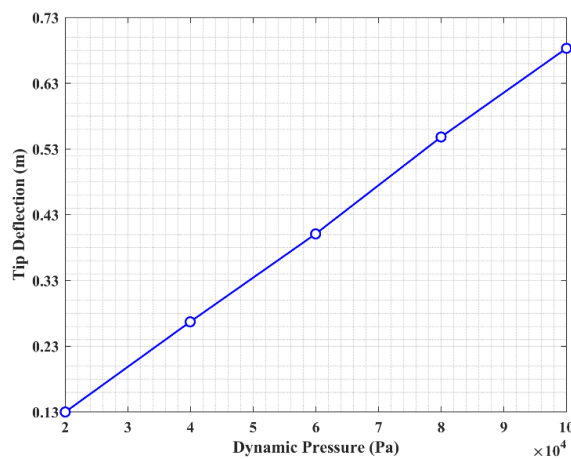


Figure 9. Dynamic pressure vs tip deflection

The lower bending moment at the free end, on the other hand, induces a smaller bending deformation, resulting in a smaller deflection at that end. The variation of the torsional angle at the obtained divergence speed along the span is shown in Figure 10 for the slender wing.

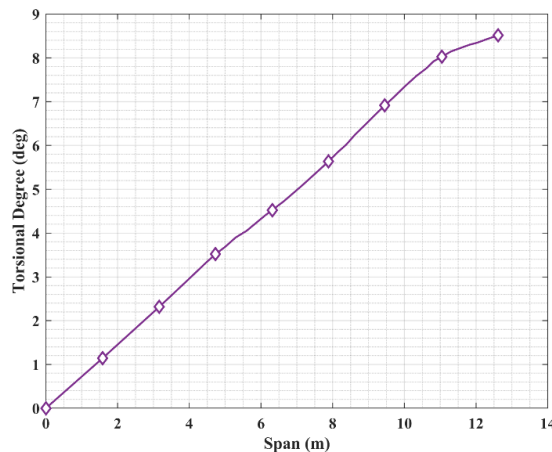


Figure 10. Wing span vs torsional angle

Flutter, an instability phenomenon, arises when aerodynamic forces interact with structural dynamics, inducing oscillations and potential failure. Figure 11 indicates that flutter speed diminishes with increasing sweep angle and wing span. This trend arises due to the sweep angle's influence on aerodynamic force distribution across the wing and the wing span's impact on the structure's natural frequencies and mode shapes, collectively heightening susceptibility to flutter.

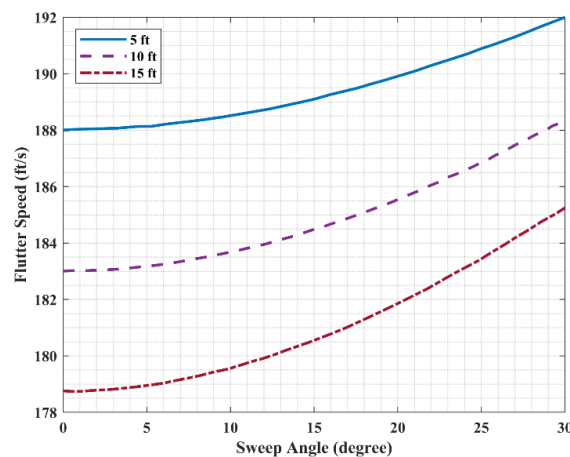


Figure 11. Flutter speed vs sweep angle

The damping ratio serves as an indicator of energy dissipation within a system. The figure.12 indicates a decrease in flutter speed with increasing damping ratio and wing span. This correlation arises from the fact that a lower damping ratio signifies a reduced capacity for dissipating energy caused by aerodynamic forces. Additionally, the wing span influences the structure's natural frequencies and mode shapes, contributing to heightened susceptibility to flutter.

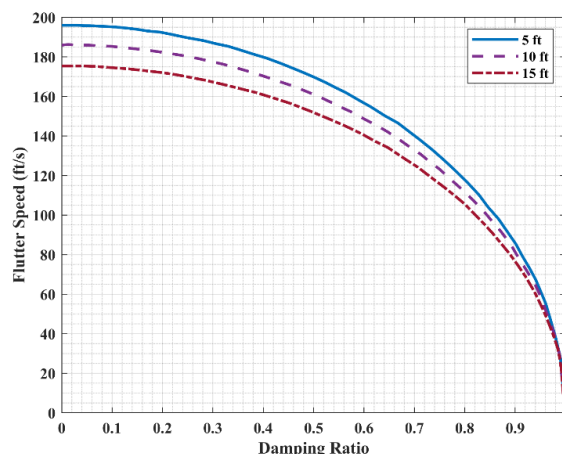


Figure 12. Flutter vs damping ratio

Figure 13 shows the variation of the distance between the elastic axis and aerodynamic axis along the chord (e) vs flutter speed. Flutter is an instability that occurs when the aerodynamic forces on a structure interact with its structural dynamics, causing it to oscillate and potentially fail. The plot demonstrates that the flutter speed increases as the value of e increases. This is because a higher value of e means that the elastic axis is further from the aerodynamic axis, which can lead to increased torsional stiffness and decreased susceptibility to flutter.

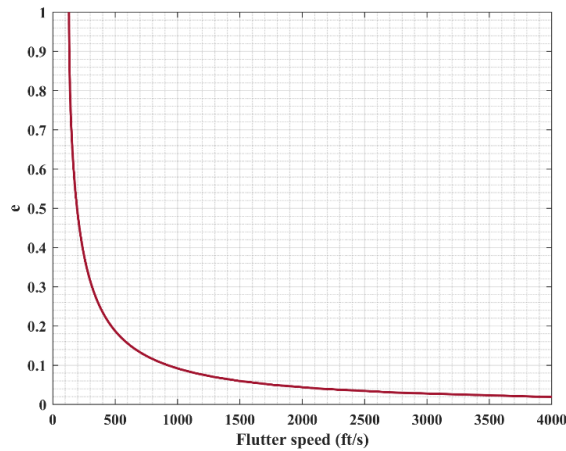


Figure 13. Variation of e vs flutter speed

Figure 14 demonstrates that the flutter frequency increases with flight speed for all three wing spans. This is because the aerodynamic forces on the wing increase with flight speed, which can lead to increased bending and twisting of the wing, and ultimately, flutter. The graph also shows that the flutter frequency decreases with wing span for all values of flight speed. This is because a larger wing span means that the wing is more flexible, which can lead to lower natural frequencies and increased susceptibility to flutter.

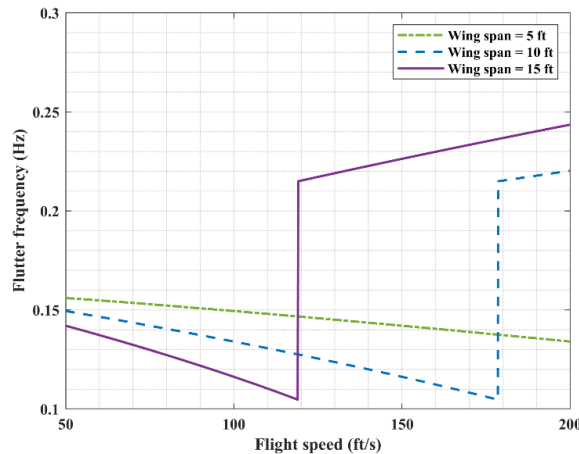


Figure 14. Flutter frequency vs flutter speed

Figure 15 shows the displacement of two different modes of vibration over time at the maximum flutter speed calculated by the code. The two modes are determined by the eigenvalues and eigenvectors of the p - k matrix, which describes the aeroelastic behavior of the wing. The mode with the higher frequency (Mode 2) has a shorter period and a higher frequency than the mode with the lower frequency (Mode 1). The displacement of each mode is shown as a function of time, with time on the x -axis and displacement on the y -axis. The displacement is measured in feet and represents the amount of deflection of the wing due to the aeroelastic forces acting on it.

Figure 16 shows how the flutter speed of a wing changes with altitude. The blue line represents the flutter speed, which increases as altitude increases due to the decrease in air density. The red dashed line represents the design flutter speed, and the green dashed line represents the design flutter speed plus 15%, which is a safety margin. The plot helps to ensure that the wing is designed to withstand the expected aerodynamic forces at different altitudes.

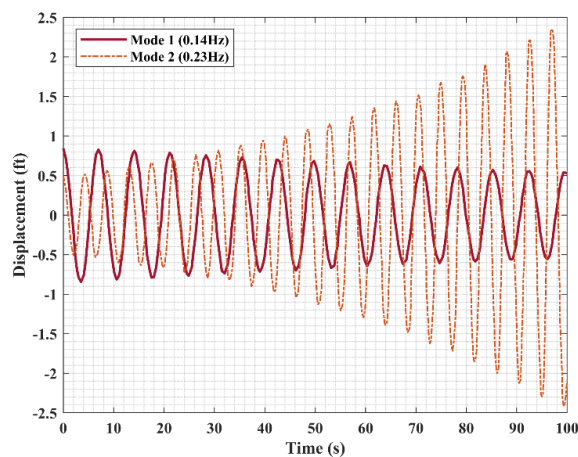


Figure 15. Displacement vs time

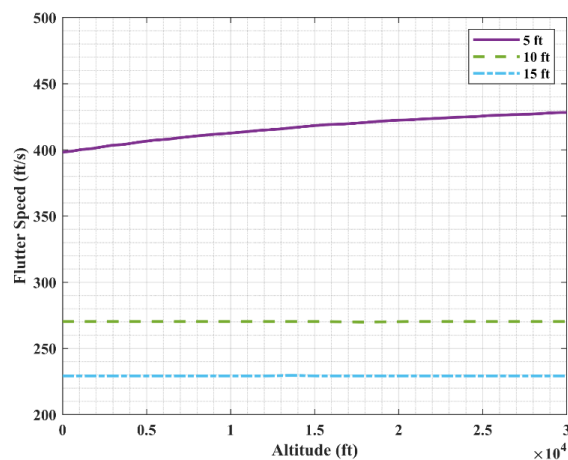


Figure 16. Flutter speed vs altitude

4.0 CONCLUSION

The divergence and flutter speeds of a system serve as crucial parameters that play a pivotal role in determining the system's stability and safety. The alteration of various parameters can exert a significant influence on these speeds, underscoring the importance of comprehending the impact of these parameters on the behavior of the system. This research delves into the repercussions of modifications in lift curve slope, span, and sweep on the divergence and flutter speeds exhibited by a system. A computational and numerical approach has been devised utilizing MATLAB and ANSYS to conduct static aeroelastic and flutter analyses on a slender straight wing. The equilibrium equations governing the system have been effectively addressed by establishing a pertinent relationship between twist and elastic lift coefficient through strip theory, incorporating both finite span correction and its absence. In the flutter analysis, the equation of motion was tackled by employing the P-k method in conjunction with Theodorsen aerodynamics. The divergence speed derived from the MATLAB code demonstrates favorable consistency with the results derived from computational fluid dynamics (CFD) analysis. The flutter results have been cross-validated with existing literature. In summary, the findings suggest that the divergence speed ascertained through strip theory with finite span correction stands at 532 m/s. Introducing a change in the lift-curve slope results in an 8% escalation in the divergence speed, culminating in a wing divergence speed of 568 m/s. It indicates that the strip theory without finite span correction can be used to understand the order of the divergence speed while the strip theory with finite span correction yields a more conservative result. Elastic axis location plays an important role in determining the divergence speed. As the fraction of chord increases by 0.5, the divergence speed increases by 13% and it is 562.17m/s w.r.t lift-curve slope. As the Mach number increases, the effectiveness of the control surface diminishes. This phenomenon is attributed to heightened compressibility effects that disrupt the flow, leading to a reduction in the lift generated by the control surface. Ansys FSI could be used to obtain the divergence dynamic pressure along with the deflection produced due to elastic twist, which shows huge deformation when the wing approaches its divergence dynamic pressure.

In the field of aeroelasticity, flutter is a dynamic phenomenon that arises when the natural frequency of a wing coincides with the frequency of the airflow surrounding it. Various parameters, such as the separation between the elastic axis and aerodynamic axis, the wing's span, and its sweep, collectively influence the occurrence of flutter. In this research article, we have investigated the impact of these parameters on the flutter speed of a slender wing. Our findings shed light

on the complex interplay between structural and aerodynamic factors that contribute to the onset of flutter and provide valuable insights for the design and optimization of aircraft structures.

In conclusion, our research has shown that the flutter speed of a wing is primarily dependent on its eccentricity, with a decrease in 'e' resulting in a 1.5% increase in flutter speed at the onset and an exponential increase as 'e' is further decreased. Additionally, we found that for a wing with a 15ft span, an increase in sweep angle from 15-30 degrees resulted in a 2.54% increase in flutter speed. Furthermore, we observed that for wings with a span of 5ft-15ft, there was a 5% increase in flutter speed, although this percentage may vary depending on other parameters such as 'e' and span. These findings provide valuable insights into the factors that influence flutter speed and can inform the design of more efficient and stable wings for various applications.

5.0 ACKNOWLEDGEMENT

The authors would like to thank the management of the Bharath Institute of Higher Education and Research, Chennai, India for their support. This study was not supported by any grants from funding bodies in the public, private, or not-for-profit sectors.

6.0 CONFLICT OF INTEREST

The authors declare no conflicts of interest

7.0 REFERENCES

- [1] P. C. Chen, D. D. Liu, and D. Sarhaddi, "High-order vs low-order panel methods for unsteady subsonic lifting surfaces," *Journal of Aircraft*, vol. 41, no. 4, pp. 957–959, 2004.
- [2] C. Yang, B. Zhang, Z. Wan, and Y. Wang, "A method for static aeroelastic analysis based on the high-order panel method and modal method," *Science China. Technological Sciences*, vol. 54, no. 3, pp. 741–748, 2011.
- [3] S. Malik, S. Ricci, and L. Riccobene, "Aeroelastic analysis of a slender wing," *CEAS Aeronautical Journal*, vol. 11, no. 4, pp. 917–927, 2020.
- [4] M. Nowak, "Improved aeroelastic design through structural optimization," *Bulletin of the Polish Academy of Sciences-technical Sciences*, vol. 60, no. 2, pp. 237–240, 2012.
- [5] C. Huang, J. Huang, X. Song, G. Zheng, and G. Yang, "Three dimensional aeroelastic analyses considering free-play nonlinearity using computational fluid dynamics/computational structural dynamics coupling," *Journal of Sound and Vibration*, vol. 494, p. 115896, 2021.
- [6] C. Huang, J. Huang, X. Song, G. Zheng, and X. Nie, "Aeroelastic simulation using CFD/CSD coupling based on precise integration method," *International Journal of Aeronautical and Space Sciences*, vol. 21, no. 3, pp. 750–767, 2020.
- [7] A. S. Thelen, L. Leifsson, and P. S. Beran, "Aeroelastic flutter prediction using multi-fidelity modeling of the aerodynamic influence coefficients," *AIAA Scitech 2019 Forum*, 2019.
- [8] Y. Chai, W. Gao, B. Ankay, F. Li, and C. Zhang, "Aeroelastic analysis and flutter control of wings and panels: A review," *International Journal of Mechanical System Dynamics*, vol. 1, no. 1, pp. 5–34, 2021.
- [9] M. R. Chiarelli and S. Bonomo, "Numerical Investigation into Flutter and Flutter-Buffer Phenomena for a Swept Wing and a Curved Planform Wing," *International Journal of Aerospace Engineering*, vol. 2019, pp. 1–19, 2019.
- [10] E. C. Culler and J. Farnsworth, "Higher frequencies in stall flutter moment development," *Journal of Fluids and Structures*, vol. 85, pp. 181–198, 2019.
- [11] A. Jameson, "Time dependent calculations using multigrid, with applications to unsteady flows past airfoils and wings," *10th Computational Fluid Dynamics Conference*, vol. 1991–1596, 1991.
- [12] W. R. Krüger, T. Klimmek, R. Liepelt, H. Schmidt, S. Waitz, and S. Cumnantip, "Design and aeroelastic assessment of a forward-swept wing aircraft," *CEAS Aeronautical Journal*, vol. 5, no. 4, pp. 419–433, 2014.
- [13] P. Camacho, H. Akhavan, and P. Ribeiro, "Linear aeroelastic analysis of cantilever hybrid composite laminated plates with curvilinear fibres and carbon nanotubes," *Composite Structures*, vol. 266, p. 113765, 2021.
- [14] S. Haghghat, J. R. R. A. Martins, and H. H. T. Liu, "Aeroservoelastic design optimization of a flexible wing," *Journal of Aircraft*, vol. 49, no. 2, pp. 432–443, 2012.
- [15] P. D. Dunning, B. Stanford, and H. A. Kim, "Level-set topology optimization with aeroelastic constraints," *56th AIAA/ASCE/AHS/ASC Structures, Structural Dynamics, and Materials Conference*, 2015.
- [16] J. S. Przemieniecki, "matrix structural analysis of substructures," *AIAA Journal*, vol. 1, no. 1, pp. 138–147, 1963.
- [17] J. Yang, Y. Liu, and W. Zhang, "Static aeroelastic modeling and rapid analysis of wings in transonic flow," *International Journal of Aerospace Engineering*, vol. 2018, pp. 1–12, 2018.

- [18] Y. Ouyang, K. Zeng, X. Kou, Y. Gu, and Z. Yang, “Experimental and numerical studies on static aeroelastic behaviours of a Forward-Swept wing model,” *Shock and Vibration*, vol. 2021, pp. 1–12, 2021.
- [19] E. C. Culler, C. Fagley, J. Seidel, T. McLaughlin, and J. Farnsworth, “Developing a reduced order model from structural kinematic measurements of a flexible finite span wing in stall flutter,” *Journal of Fluids and Structures*, vol. 71, pp. 56–69, 2017.
- [20] J. Tran, H. Gao, J. Sirohi, and M. Wei, “Reduced-order methodology for prediction of loads generated by a flexible flapping wing,” *International Journal of Micro Air Vehicles (Print)*, vol. 10, no. 1, pp. 31–41, 2017.
- [21] M. Tatar and M. H. Sabour, “Reduced-order modeling of dynamic stall using neuro-fuzzy inference system and orthogonal functions,” *Physics of Fluids*, vol. 32, no. 4, 2020.
- [22] G. C. Silva, M. V. Donadon, and F. J. Silvestre, “Experimental and numerical investigations on the nonlinear aeroelastic behavior of high aspect-ratio wings for different chord-wise store positions under stall and follower aerodynamic load models,” *International Journal of Nonlinear Mechanics*, vol. 131, p. 103685, 2021.
- [23] S. Jayatilake and B. Titurus, “Nonlinear aeroelastic analysis of a damped elastica-aerofoil system,” *Nonlinear Dynamics*, vol. 109, no. 2, pp. 731–754, 2022.
- [24] S. A. Fazlzadeh, M. Rezaei, and A. Mazidi, “Aeroelastic analysis of swept pre-twisted wings,” *Journal of Fluids and Structures*, vol. 95, p. 103001, 2020.
- [25] M. F. Westin, J. M. Balthazar, R. G. A. Da Silva, M. A. Ribeiro, and Â. M. Tuset, “Characterization of aeroelastic behavior in a high aspect ratio wing using computational and wind tunnel experiments,” *Axioms*, vol. 12, no. 9, p. 826, 2023.
- [26] Q. Yu, M. Damodaran, and B. C. Khoo, “Predicting wing-pylon-nacelle configuration flutter characteristics using adaptive continuation method,” *Advances in Aerodynamics*, vol. 5, no. 1, 2023.
- [27] Q. Yu, M. Damodaran, and B. C. Khoo, “Nonlinear airfoil limit cycle analysis using continuation method and filtered impulse function,” *AIAA Journal (Print)*, vol. 58, no. 5, pp. 1976–1991, 2020.
- [28] Q. Yu, M. Damodaran, and B. C. Khoo, “Nonlinear aeroelastic analysis of a multi-element airfoil with free play using continuation method,” *Journal of Fluids and Structures*, vol. 109, p. 103482, 2022.
- [29] “Solve system of nonlinear equations - MATLAB fsolve - MathWorks United Kingdom.” <https://uk.mathworks.com/help/optim/ug/fsolve.html>
- [30] R. L. Bisplinghoff, H. Ashley, and R. L. Halfman, *Aeroelasticity*. Dover Publications, Mineolo, NY, USA 2013.
- [31] D. H. Hodges and G. A. Pierce, *Introduction to structural dynamics and aeroelasticity*. Cambridge University Press, Cape town, South Africa, 2011.
- [32] A. E. H. Love, *A treatise on the mathematical theory of elasticity*. Cambridge University Press, 2013.